# Acoustic and optical phonon scattering of the 1*S* yellow orthoexciton in $Cu_2O$

G. Baldassarri Höger von Högersthal,* D. Fröhlich,† M. Kulka, Th. Auer, and M. Bayer
*Institut für Physik, Universität Dortmund, D-44221 Dortmund, Germany*

H. Stolz
*Fachbereich Physik, Universität Rostock, D-18051 Rostock, Germany*
(Received 13 September 2005; published 4 January 2006)

Resonant Raman measurements have been performed on the 1*S* yellow orthoexciton in $Cu_2O$ in high magnetic field. At zero field, the $\Gamma_3^-$, $\Gamma_4^-$, and $\Gamma_5^-$ phonon replicas are visible. In magnetic field we observe a characteristic fine structure in the optical phonon replicas. It is explained by longitudinal and transversal acoustic phonon scattering of orthoexcitons between different Zeeman components. We derive in detail the polarization dependence of the phonon sidebands for these exciton components. For the dipole-allowed $\Gamma_4^-$ phonon we take the splitting into longitudinal and transverse phonons into account. There is good agreement with the experimental results confirming the importance of a $\vec{k}$-dependent exciton mass for understanding relaxation processes.

DOI: 10.1103/PhysRevB.73.035202 PACS number(s): 78.20.−e, 78.40.Fy, 78.30.−j, 71.36.+c

## I. INTRODUCTION

Resonant optical phonon scattering from excitons in $Cu_2O$ was extensively studied in the past.[1,2] There are, however, only few experiments on acoustic phonon scattering.[2] Acoustic phonon scattering from the lowest 1*S* exciton is of special interest in connection with relaxation processes into polariton states which might inhibit Bose-Einstein condensation of the lowest quadrupole allowed exciton as discussed in Ref. 3. With respect to Bose-Einstein condensation (BEC) in $Cu_2O$, our investigations are at least interesting in the following two aspects. (i) With the splitting in a magnetic field the degeneracy of the threefold orthoexciton is lifted which raises the critical temperature for BEC. (ii) The detailed study of acoustic phonon scattering together with the study of its field dependence allows a more profound understanding of exciton-phonon interaction and might open possibilities for tailoring relaxation processes in order to cool down the exciton system.

As was first shown for GaAs,[4] resonant Brillouin scattering is a powerful tool to study acoustic phonon scattering. For the lowest exciton series in $Cu_2O$ resonant Brillouin scattering is allowed for *P* excitons as was shown in Ref. 5, but for the 1*S* exciton in $Cu_2O$ it is parity forbidden for electric dipole emission. Electric quadrupole emission is expected to be too weak to be detected close to the quadrupole exciting laser line.

We report on an alternative method to study in detail acoustic phonon scattering within the lowest threefold 1*S* orthoexciton in $Cu_2O$. An additional odd-parity optical phonon of $\Gamma_3^-$, $\Gamma_4^-$, or $\Gamma_5^-$ symmetry allows one to detect acoustic phonon scattering as was already shown in Ref. 2. Applying a magnetic field splits the threefold orthoexciton of $\Gamma_5^+$ symmetry into three components ($M=0$ and $M=\pm 1$). Intra- and interband acoustic phonon scattering lead to a rich spectrum of resonances which will be analyzed by their polarization dependence for different wave vector and magnetic field configurations.

For the analysis it was necessary to extend the quadrupole Raman selection rules of Ref. 6 in three aspects. (i) The selection rules are derived separately for the three Zeeman components including circular polarization. (ii) The selection rules are generalized to include optical phonon emission from each Zeeman component, independently of its excitation either by direct quadrupole absorption as in Ref. 6 or indirectly by acoustic phonon scattering from another quadrupole excited component. (iii) The selection rules for the $\Gamma_4^-$ phonon polariton distinguish the scattering by longitudinal optical (LO) and transverse optical (TO) phonons for any phonon *q* vector.

The paper is organized as follows. In Sec. II, we will derive the selection rules as stated above, where it is essential to take into account the $\vec{k}$-dependent exchange terms as discussed recently.[7] After a short description of the experimental setup in Sec. III, we present in Sec. IV the experimental results and their discussion. In the last section we present conclusions with an outlook on further investigations.

## II. THEORY

In the following we address the magnetic field splitting of the orthoexciton and the Raman selection rules. As discussed in detail in Ref. 7, the yellow 1*S* orthoexciton in $Cu_2O$ has $\Gamma_5^+$ symmetry and is split by $k^2$-exchange terms into three components. In an external magnetic field *B*, one has to include the field-induced interaction of the orthoexciton with the paraexciton of $\Gamma_2^+$ symmetry, which is shifted by $\epsilon = 12.11$ meV to lower energy by short-range isotropic exchange interaction.[8] In the $\Gamma_2^+$, $\Gamma_{5x}^+$, $\Gamma_{5y}^+$, $\Gamma_{5z}^+$ basis, the magnetic field interaction matrix is given by

 

$$\boldsymbol{H}_B(\vec{B}) = \begin{bmatrix} -\varepsilon & i\alpha B_x & i\alpha B_y & i\alpha B_z \\ -i\alpha B_x & 0 & -i\beta B_z & i\beta B_y \\ -i\alpha B_y & i\beta B_z & 0 & -i\beta B_x \\ -i\alpha B_z & -i\beta B_y & i\beta B_x & 0 \end{bmatrix}, \quad (1)$$

where $\alpha = 92.5\ \mu$eV/T and $\beta = 47.7\ \mu$eV/T are the Zeeman parameters for the fourfold yellow $1S$ exciton in $Cu_2O$ and $B_i$ $(i=x,y,z)$ are the magnetic field components with respect to the crystalline axes. Diagonalization of the interaction matrix leads to a splitting of the $\Gamma_5^+$ orthoexciton into three components $M=\pm 1$ and $M=0$ and a field-induced repulsion of the $\Gamma_2^+$ paraexciton and the $M=0$ component.[8–10]

Recently it was shown by high-resolution spectroscopy[7] that even without external perturbation, like a magnetic field, the $1S$ yellow exciton of $\Gamma_5^+$ symmetry is not threefold degenerate any more but split into up to three components. This splitting depends on the exciton wave vector $\vec{k}$. For a high-symmetry direction like $\vec{k} \| [001]$ the exciton is split into a doublet and a singlet with $\Delta E = 4\ \mu$eV and for a lower-symmetry direction like $\vec{k} \| [110]$ the degeneracy is fully lifted. This splitting is due to $k^2$-exchange terms. As discussed in detail in Ref. 7 the $\vec{k}$-dependent electron-hole exchange of the orthoexciton can be described in the Hamiltonian $\boldsymbol{H}_{ex}(\vec{k})$ by four $3\times 3$ matrices with the parameters $\Delta_1 = -8.6\ \mu$eV, $\Delta_3 = -1.3\ \mu$eV, $\Delta_5 = 2\ \mu$eV, and $\Delta_Q = 5\ \mu$eV. In order to include the paraexciton, the exchange matrices have to be augmented by adding a row and a column with zeros, because the paraexciton is not affected by the exchange terms.[11] Neglecting polaritonic effects, we get the band dispersions of the three orthoexciton components and the paraexciton from the diagonalization of the Hamiltonian:

$$\boldsymbol{H}(\vec{k}) = \boldsymbol{H}_{kin}(k^2) + \boldsymbol{H}_{ex}(\vec{k}) + \boldsymbol{H}_B(\vec{B}). \quad (2)$$

$\boldsymbol{H}_{kin}(k^2)$ describes the kinetic energy term of the exciton with the mass parameter $M_0 = m_e + m_h = 1.64 m_0$.[7,11,12] Though the splitting due to the $k^2$-exchange terms is small (a few $\mu$eV at resonance $k_0$) as compared to the magnetic field splitting (100 $\mu$eV at 2 T), these terms lead to an anisotropic mass and thus to characteristic exciton dispersion curves for the magnetic field components.

We now derive the selection rules for the $\Gamma_3^-$, $\Gamma_4^-$, and $\Gamma_5^-$ phonon emission from the three magnetic-field-split components $M=0,\pm 1$ of the $\Gamma_5^+$ orthoexciton. Birman[6] has derived the quadrupole Raman selection rules for these phonons for the threefold-degenerate $\Gamma_5^+$ exciton. However, we do not restrict ourselves to the quadrupole-allowed components, but we will extend the calculations of Birman[6] to the optical phonon emission ($\Gamma_3^-$, $\Gamma_4^-$, and $\Gamma_5^-$ phonons) from the other components ($M=\pm 1$), which are, as shown in Fig. 1, not directly excited but coupled by acoustic phonon interaction (Stokes and anti-Stokes processes) to the quadrupole excited $M=0$ component. One might term these processes as two-phonon Raman scattering as discussed in detail for the $B=0$ T case in Ref. 2. As a first case we will consider the $\Gamma_3^-$ optical phonon emission for a magnetic field in the [110] direction. From the diagonalization of the matrix [Eq. (1)] we get in the basis $\Gamma_{5x}^+$, $\Gamma_{5y}^+$, $\Gamma_{5z}^+$ for the eigenvectors

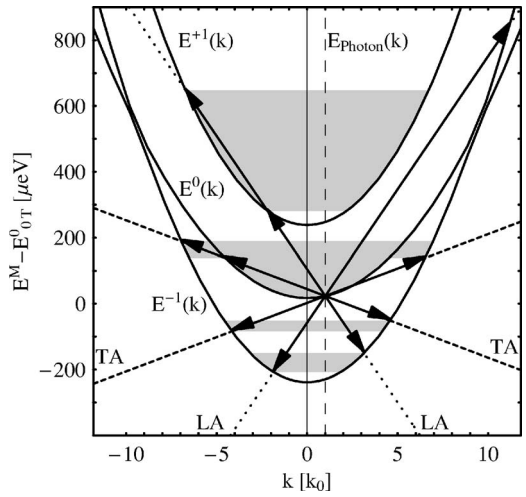


FIG. 1. Energy dispersion $E^M$ of the $M=0,\pm 1$ orthoexciton components at 5 T for $\vec{k} \| [1\bar{1}0]$, $\vec{B} \| [110]$ (solid lines) relative to the energy of the $M=0$ component at 0 T, $E_{0T}^0$. Dashed (dotted) lines refer to TA (LA) acoustic phonon dispersions starting at $E_{5T}^0(k_0)$. The vertical dashed line at $k=k_0$ refers to the photon dispersion. $k$ values are given in units of the resonance wave number $k_0 = 2.62 \times 10^7\ \mathrm{m}^{-1}$. Arrows highlight possible scattering processes. Gray shaded areas show the energy ranges of possible scattering processes.

$$|M=0\rangle = \frac{1}{\sqrt{2}}\begin{pmatrix} 1 \\ 1 \\ 0 \end{pmatrix},$$

$$|M=+1\rangle = \frac{1}{2}\begin{pmatrix} -i \\ i \\ \sqrt{2} \end{pmatrix},$$

$$|M=-1\rangle = \frac{1}{2}\begin{pmatrix} i \\ -i \\ \sqrt{2} \end{pmatrix}. \quad (3)$$

For the discussion of selection rules we can neglect the coupling of the $|M=0\rangle$ component to the paraexciton $|\Gamma_2^+\rangle$ and the mixing of the $\Gamma_5^+$ components due to the $k^2$-exchange terms. With use of the contracted scattering tensors (Table 1 for $\Gamma^{12-}$ from Ref. 6) or the tables of Koster *et al.*[13] one can calculate the relative oscillator strength for any polarization $\vec{e}_i$ of the outgoing light and component $M$ of the $\Gamma_5^+$ orthoexciton [Eq. (3)]. For the magnetic field in the [110] direction we choose the following polarization vectors for the outgoing light:

$$\vec{e}_1 = (0,0,1), \quad \vec{e}_2 = \frac{1}{\sqrt{2}}(1,-1,0), \quad \vec{e}_3 = \frac{1}{\sqrt{2}}(1,1,0),$$

$$\vec{e}_4 = \frac{1}{\sqrt{2}}(\vec{e}_1 + i\vec{e}_2), \quad \vec{e}_5 = \frac{1}{\sqrt{2}}(\vec{e}_1 - i\vec{e}_2). \tag{4}$$

The oscillator strength of emission of light with polarization $\vec{e}_i$ and a phonon $\Gamma_3^-$ from the component $M$ is given by

$$OM_{3i} = \sum_{j=1}^{2} |\vec{e}_i^{\,*} \cdot \boldsymbol{\sigma}_j^3 \cdot \vec{M}|^2. \tag{5}$$

The matrices $\boldsymbol{\sigma}_1^3$ and $\boldsymbol{\sigma}_2^3$ are taken from Table 1 of Ref. 6 with correction of a sign in $\boldsymbol{\sigma}_2^3$:

$$\boldsymbol{\sigma}_1^3 = \frac{\beta}{\sqrt{2}}\begin{pmatrix} 1 & 0 & 0 \\ 0 & -1 & 0 \\ 0 & 0 & 0 \end{pmatrix}, \quad \boldsymbol{\sigma}_2^3 = \frac{\beta}{\sqrt{6}}\begin{pmatrix} 1 & 0 & 0 \\ 0 & 1 & 0 \\ 0 & 0 & -2 \end{pmatrix}. \tag{6}$$

For example, for $M=0$ and $\vec{e}_2$ we get $O0_{32}=\beta^2/2$, the parameter $\beta$ being a measure of the interaction strength.

For the $\Gamma_5^-$ phonon there are three phonon matrices[6] $\boldsymbol{\sigma}_i^5$ $(i=1-3)$ in Eq. (5):

$$\boldsymbol{\sigma}_1^5 = \frac{\delta}{\sqrt{2}}\begin{pmatrix} 0 & 0 & 0 \\ 0 & 0 & 1 \\ 0 & -1 & 0 \end{pmatrix}, \quad \boldsymbol{\sigma}_2^5 = \frac{\delta}{\sqrt{2}}\begin{pmatrix} 0 & 0 & -1 \\ 0 & 0 & 0 \\ 1 & 0 & 0 \end{pmatrix},$$

$$\boldsymbol{\sigma}_3^5 = \frac{\delta}{\sqrt{2}}\begin{pmatrix} 0 & 1 & 0 \\ -1 & 0 & 0 \\ 0 & 0 & 0 \end{pmatrix}. \tag{7}$$

Of special interest is the $\Gamma_4^-$ phonon, since it is dipole allowed and thus expected to split into transverse and longitudinal components. In the following we will derive for a general direction $\vec{q}$ of the $\Gamma_4^-$ phonon wave vector the polarization selection rules separately for the longitudinal and transverse phonons. We first define the longitudinal $(\vec{q})$ and the two transverse ($\vec{t}$ and $\vec{s}$) phonon polarization vectors:

$$\vec{q} = (q_1, q_2, q_3),$$

$$\vec{t} = \left(1 - \frac{q_1^2}{1+q_3}, \frac{-q_1 q_2}{1+q_3}, -q_1\right),$$

$$\vec{s} = \left(\frac{-q_1 q_2}{1+q_3}, 1 - \frac{q_2^2}{1+q_3}, -q_2\right). \tag{8}$$

With use of the $\Gamma_4^-$ phonon matrices from Ref. 6

$$\boldsymbol{\sigma}_1^4 = \frac{\gamma}{\sqrt{2}}\begin{pmatrix} 0 & 0 & 0 \\ 0 & 0 & 1 \\ 0 & 1 & 0 \end{pmatrix}, \quad \boldsymbol{\sigma}_2^4 = \frac{\gamma}{\sqrt{2}}\begin{pmatrix} 0 & 0 & 1 \\ 0 & 0 & 0 \\ 1 & 0 & 0 \end{pmatrix},$$

$$\boldsymbol{\sigma}_3^4 = \frac{\gamma}{\sqrt{2}}\begin{pmatrix} 0 & 1 & 0 \\ 1 & 0 & 0 \\ 0 & 0 & 0 \end{pmatrix}, \tag{9}$$

and the phonon polarization vectors [Eq. (8)] we now determine the phonon matrices for the longitudinal ($\boldsymbol{L}$) and the transverse phonons ($\boldsymbol{T}$) and ($\boldsymbol{S}$):

$$\boldsymbol{L} = q_1\boldsymbol{\sigma}_1^4 + q_2\boldsymbol{\sigma}_2^4 + q_3\boldsymbol{\sigma}_3^4,$$

$$\boldsymbol{T} = t_1\boldsymbol{\sigma}_1^4 + t_2\boldsymbol{\sigma}_2^4 + t_3\boldsymbol{\sigma}_3^4,$$

$$\boldsymbol{S} = s_1\boldsymbol{\sigma}_1^4 + s_2\boldsymbol{\sigma}_2^4 + s_3\boldsymbol{\sigma}_3^4. \tag{10}$$

The oscillator strength for light emission with polarization $\vec{e}_i$ from the component $M$ has to be calculated separately for longitudinal and transverse $\Gamma_4^-$ phonons:

$$OM_{4Li} = |\vec{e}_i^{\,*} \cdot \boldsymbol{L} \cdot \vec{M}|^2,$$

$$OM_{4Ti} = |\vec{e}_i^{\,*} \cdot \boldsymbol{T} \cdot \vec{M}|^2 + |\vec{e}_i^{\,*} \cdot \boldsymbol{S} \cdot \vec{M}|^2. \tag{11}$$

For the magnetic field along [001], the $M$ components are given by

$$|M=0\rangle = \begin{pmatrix} 0 \\ 0 \\ 1 \end{pmatrix},$$

$$|M=+1\rangle = \frac{1}{\sqrt{2}}\begin{pmatrix} 1 \\ i \\ 0 \end{pmatrix},$$

$$|M=-1\rangle = \frac{1}{\sqrt{2}}\begin{pmatrix} 1 \\ -i \\ 0 \end{pmatrix}. \tag{12}$$

The polarization vectors $\vec{e}_i$ are now chosen as

$$\vec{e}_1 = \frac{1}{\sqrt{2}}(1,-1,0), \quad \vec{e}_2 = \frac{1}{\sqrt{2}}(1,1,0), \quad \vec{e}_3 = (0,0,1),$$

$$\vec{e}_4 = \frac{1}{\sqrt{2}}(\vec{e}_1 + i\vec{e}_2), \quad \vec{e}_5 = \frac{1}{\sqrt{2}}(\vec{e}_1 - i\vec{e}_2). \tag{13}$$

In Table I we present our results for two directions of the magnetic field ([110] and [001]) and different polarization vectors of detected light; for the $\Gamma_4^-$ phonon, the reported values refer to the direction $\vec{q}$ of the phonon momentum parallel to the laser wave vector $\vec{k}$ (e.g., forward and backward Raman scattering). Our results apply to Voigt and Faraday configurations depending on the choice of the $\vec{k}$ vector of the exciting laser relative to the magnetic field direction. For $\Gamma_4^-$ phonons the results in Table I refer to Voigt configuration. The amplitudes for the quadrupole transition to the $M$ components [Eqs. (3) and (12)] for any $\vec{e}_i$ and $\vec{k}$ vector perpendicular to $\vec{e}_i$ are calculated taking the scalar product of the relevant $M$ vector with the vector $\vec{a}_i$, where $\vec{a}_i$ is given by the symmetric vector product of $\vec{e}_i$ and $\vec{k}$:[7]

$$\vec{a}_i = \begin{pmatrix} e_{iy}k_z + e_{iz}k_y \\ e_{iz}k_x + e_{ix}k_z \\ e_{ix}k_y + e_{iy}k_z \end{pmatrix}. \tag{14}$$

The dipole selection rules for the outgoing photons are then determined as outlined above.

TABLE I. Oscillator strength for optical phonon emission ($\Gamma_3^-$, $\Gamma_5^-$, and $\Gamma_4^-$ phonons) from orthoexciton components $M=0,\pm1$ (first column) in units of $\beta^2$, $\gamma^2$, and $\delta^2$ for linearly and circularly polarized light and $\vec{B}\|[110]$ and $[001]$; for $\Gamma_4^-$ phonons, the values refer to a $\vec{q}$ direction of phonon momentum parallel to laser wave vector $\vec{k}$, as indicated.

| | $\vec{B}\|[110]$ | | | $\vec{B}\|[001]$ | | | | | | |
|---|---|---|---|---|---|---|---|---|---|---|
| | Polarization | | | | | | | | | |
| | $[001]$ | $[1\bar{1}0]$ | $[110]$ | $\sigma^+$ | $\sigma^-$ | $[1\bar{1}0]$ | $[110]$ | $[001]$ | $\sigma^+$ | $\sigma^-$ |
| $\Gamma_3^-$ | | | | | | | | | | |
| $M=0$ | 0 | 1/2 | 1/6 | 1/4 | 1/4 | 0 | 0 | 2/3 | 0 | 0 |
| $M=+1$ | 1/3 | 1/12 | 1/4 | 1/24 | 3/8 | 1/3 | 1/3 | 0 | 1/6 | 1/2 |
| $M=-1$ | 1/3 | 1/12 | 1/4 | 3/8 | 1/24 | 1/3 | 1/3 | 0 | 1/2 | 1/6 |
| $\Gamma_5^-$ | | | | | | | | | | |
| $M=0$ | 1/2 | 1/2 | 0 | 1/2 | 1/2 | 1/2 | 1/2 | 0 | 1/2 | 1/2 |
| $M=+1$ | 1/4 | 1/4 | 1/2 | 1/2 | 0 | 1/4 | 1/4 | 1/2 | 1/2 | 0 |
| $M=-1$ | 1/4 | 1/4 | 1/2 | 0 | 1/2 | 1/4 | 1/4 | 1/2 | 0 | 1/2 |
| $\Gamma_{4L}^-$ ($\Gamma_{4T}^-$) | | | $\vec{k}\|[001]$ | | | | | $\vec{k}\|[1\bar{1}0]$ | | |
| $M=0$ | 0 (1/2) | 0 (0) | 1/2 (0) | 0 (1/4) | 0 (1/4) | 1/2 (0) | 0 (1/2) | 0 (0) | 1/4 (1/4) | 1/4 (1/4) |
| $M=+1$ | 0 (1/4) | 1/4 (1/4) | 0 (1/4) | 1/8 (0) | 1/8 (1/2) | 0 (1/4) | 0 (1/4) | 1/4 (1/4) | 0 (0) | 0 (1/2) |
| $M=-1$ | 0 (1/4) | 1/4 (1/4) | 0 (1/4) | 1/8 (1/2) | 1/8 (0) | 0 (1/4) | 0 (1/4) | 1/4 (1/4) | 0 (1/2) | 0 (0) |

Let us now consider the acoustic phonon scattering processes in more detail. In Fig. 1 we show the $k$ dispersion of the Zeeman components for Voigt configuration with $\vec{k}\|[1\bar{1}0]$ and $B=5$ T, $\vec{B}\|[001]$. The $x$ axis is given in units of the resonant state at $k_0=2.62\times10^7$ m$^{-1}$ as defined by the photon dispersion (vertical dashed line).[7] For acoustic phonons we assume an isotropic and linear dispersion:

$$\hbar\omega_{LA(TA)}(\vec{q})=\hbar v_{LA(TA)}q, \tag{15}$$

with phonon velocities $v_{LA(TA)}=4.56(1.22)\times10^3$ m/s.[14] It was shown that this holds for $|\vec{q}|$ out to approximately one half of the Brillouin zone.[15] The system is initially excited in resonance with an $M$ component (here $M=0$ at $k=k_0$); then acoustic phonons couple the state at $k_0$ to other intra- or interband $\vec{k}$ states, as highlighted by arrows, before radiative recombination through a $\Gamma_3^-$, $\Gamma_4^-$, or $\Gamma_5^-$ optical phonon takes place. In a scattering process via acoustic phonons, energy and momentum are conserved:

$$E^0(\vec{k}_i)=E^M(\vec{k}_f)\pm\hbar\omega_{LA(TA)}(\vec{q}), \tag{16}$$

$$\vec{k}_i=\vec{k}_f\pm\vec{q}, \tag{17}$$

where + and − refer to creation (Stokes) or annihilation (anti-Stokes) of an acoustic phonon, respectively. Thus, the intersection points of the phonon dispersions with different bands define the allowed values of $\vec{k}_f$. The exciton dispersion relations are obtained from the full exciton Hamiltonian [Eq. (2)], thus including the $\vec{k}$-dependent exchange. In this simplified model the intersection points determine the extremes of the available range of $\vec{k}_f$ values for a specific configuration. In principle one should integrate the oscillator strength over all possible directions, since scattering processes take place in three dimensions (3D). This complicates the analysis especially for the $\Gamma_4^-$ phonon scattering, since one has to distinguish between LO and TO phonons for each phonon wave vector $\vec{q}$ considered in the scattering process.

## III. EXPERIMENT

In this section we briefly describe the experimental setup. For details we refer to previous publications.[7] The samples, both of 0.5 mm thickness, are cut from a high quality natural $Cu_2O$ crystal after x-ray orientation for different wave vector and thus polarization geometries. They are mounted in a strain-free condition and cooled by superfluid helium down to 1.6 K in a magneto-optical cryostat. The magnetic field is applied in Faraday or Voigt geometry with field strength up to 5 T. The Voigt configuration has the great advantage of avoiding Faraday rotation effects.

As shown in the last chapter, the $1S$ orthoexciton splits in a magnetic field into three components ($M=0,\pm1$). Excitation is provided by a single frequency dye laser with a bandwidth of about 5 neV, which is tuned into resonance with one of the Zeeman components. We report measurements for two wave vector directions, $\vec{k}$ along $[1\bar{1}0]$ and $[001]$. We have already shown that the electric quadrupole allowed orthoexciton states which can be accessed via resonant excitation depend on the photon polarization [Eq. (14)].[7] The Raman signal of the $\Gamma_3^-$ ($\Gamma_5^-$) optical phonon is shifted by 13.5 meV (10.6 meV) to lower energy (Stokes component). Our phonon energies differ for the $\Gamma_3^-$ and $\Gamma_4^-$ phonon by −0.1 meV from literature.[1,16] The $\Gamma_4^-$ phonon is split into a longitudinal (19.0 meV) and two transverse components (18.7 meV). All phonon sidebands are electric dipole allowed with linear or circular polarization, depending on the crystal orientation, as discussed in the last section.

The signal is collected in transmission or reflection geometry. The emitted light is analyzed by a polarizer, dispersed

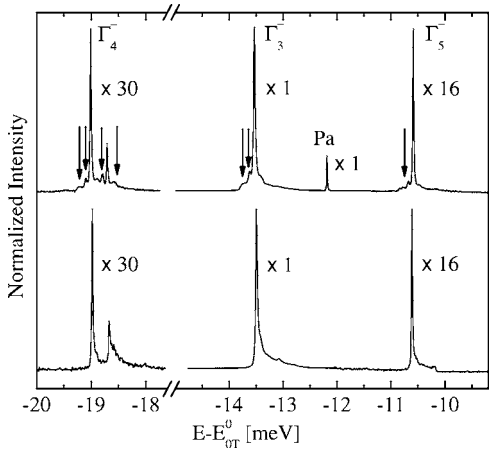


FIG. 2. Resonant Raman spectra at 1.6 K of $\Gamma_3^-$, $\Gamma_4^-$, and $\Gamma_5^-$ phonon-assisted recombination from the 1*S* yellow orthoexciton at 0 T (bottom trace) and 5 T (top trace). Excitons are excited in the $M=0$ component with $\vec{k}\|[1\bar{1}0]$, laser polarization $\vec{e}_L\|[001]$, and $\vec{B}\|[1\bar{1}0]$ (Faraday configuration). Zero energy is given relative to the $M=0$ energy at 0 T, $E_{0T}^0$. The spectra are normalized by multiplication factors as indicated in the figure. The arrows highlight the new features visible at 5 T; Pa marks the paraexciton.

by a 0.85 m Spex double monochromator working in second order and detected by a charge-coupled device camera. The spectral resolution is approximately 15 $\mu$eV.

## IV. EXPERIMENTAL RESULTS AND DISCUSSION

Figure 2 shows the Raman spectrum of one of our samples resonantly excited in the $M=0$ state with $\vec{k}\|[1\bar{1}0]$ and polarization parallel to [001] at 0 T (bottom trace) and 5 T (top trace). The sharp peaks visible at 0 T, correspond to the $\Gamma_3^-$, $\Gamma_4^-$, and $\Gamma_5^-$ phonon replicas, as confirmed by their separation from the laser excitation energy. At 5 T, the Raman peaks are shifted towards higher energy by 20 $\mu$eV, due to the corresponding *B*-induced shift of the $M=0$ state, and new features (marked by arrows) appear on both sides of each of them. Remembering that the magnetic field splits the 1*S* yellow orthoexciton level into three subbands, these experimental results suggest that there is acoustic phonon scattering from the quadrupole excited *M* component (e.g., $M=0$ for Faraday configuration with B along $[1\bar{1}0]$) to the same ($M=0$, intraband) or the other components ($M=\pm1$, interband) prior to $\Gamma_3^-$, $\Gamma_4^-$, or $\Gamma_5^-$ optical phonon emission. Due to the mixing of the paraexciton and the $M=0$ component of the orthoexciton in magnetic field, the paraexciton is quadrupole-allowed and can thus be seen for the polarization parallel to [001] (Fig. 2, top trace).

Figure 3 shows the $\Gamma_3^-$, $\Gamma_4^-$, and $\Gamma_5^-$ phonon replicas at 5 T for excitation of the $M=+1$ state with $\vec{k}\|[1\bar{1}0]$, $\vec{B}\|[001]$ (Voigt geometry), and polarization of the excitation beam parallel to the [001] direction. The detected signal is analyzed regarding polarization parallel to [001] and [110]. We first focus on the direct Raman peaks involving the $\Gamma_3^-$, $\Gamma_4^-$, or $\Gamma_5^-$ phonon, as labeled in each panel. The ratio between the

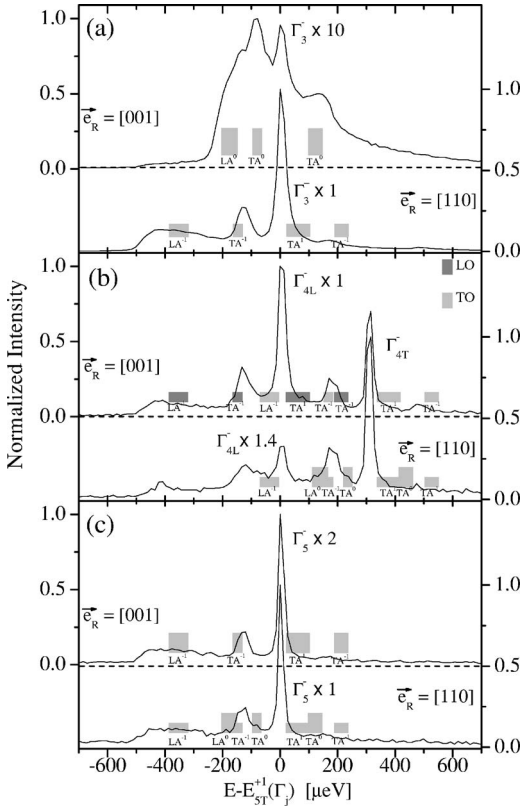


FIG. 3. $\Gamma_3^-$ (a), $\Gamma_4^-$ (b), and $\Gamma_5^-$ (c) phonon replicas at 5 T for excitation of the $M=+1$ component with $\vec{k}\|[1\bar{1}0]$, $\vec{B}\|[001]$, and polarization of the laser beam $\vec{e}_L\|[001]$. The detected signal is analyzed with polarizations $\vec{e}_R\|[001]$ (upper subpanel, left scale) and [110] (lower subpanel, right scale). Energy values are given relative to the Raman resonance of the corresponding $\Gamma_j^-$ phonon ($\Gamma_j^- = \Gamma_3^-, \Gamma_{4L}^-, \Gamma_5^-$) of the $M=+1$ component at 5 T, $E_{5T}^{+1}(\Gamma_j^-)$. $TA^i$ ($LA^i$), with $i=1,0,-1$, label peaks due to TA (LA) acoustic phonon scattering processes from the $M=+1$ state to the $M=i$ components. Height and width of shaded areas mark relative oscillator strength according to Table I and allowed energy range as indicated in Fig. 1. Dark and light shaded areas in (b) denote scattering via LO and TO phonons, respectively.

peak intensities for polarization parallel to the [110] and the [001] direction is in good agreement with the results deduced from Table I: Indeed, we observe experimental values of about 10:1, 1:6, 1:1.3, and 1:2 for the $\Gamma_3^-$, $\Gamma_{4L}^-$, $\Gamma_{4T}^-$, and $\Gamma_5^-$ phonons, respectively, to be compared with 1/3:0, 0:1/4, 1/4:1/4, and 1/4:1/2.

On both sides of the main peaks, additional features are visible, which we attribute to acoustic phonon scattering. Gray shaded areas represent the allowed ranges of scattering via LA and TA phonons as described in Sec. II. They connect the $M=+1$ component either to itself (intraband transition) or to the $M=0$, $-1$ components (interband transitions). The qualitative agreement between experiments and our simplified scattering model strongly substantiates both TA and LA acoustic phonon scattering between the orthoexciton components. The discrepancies observed in the peak energies may be ascribed to (i) the isotropic approximation of the acoustic phonon dispersions (which instead have different slopes in different directions), (ii) higher-order scattering processes in-

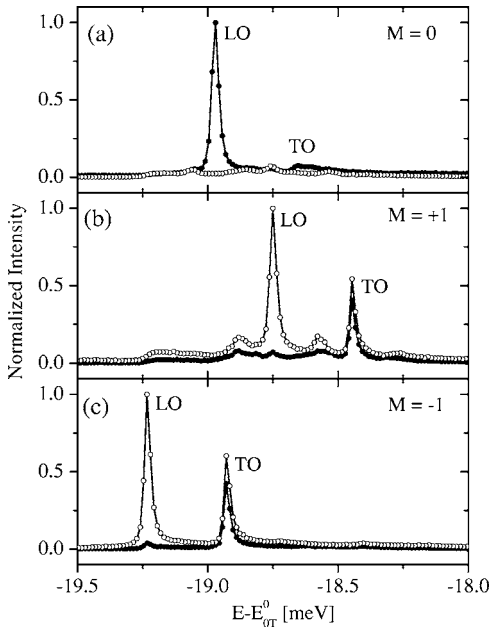


FIG. 4. Resonant Raman spectra of $\Gamma_4^-$ phonons (LO and TO) for $\vec{k}\|[001]$ and $\vec{B}\|[110]$ (Voigt configuration, $B=5$ T); full dots, Raman polarization $\vec{e}_R\|[110]$; open dots, Raman polarization $\vec{e}_R\|[1\bar{1}0]$. (a) excitation of the $M=0$ component (laser polarization $\vec{e}_L\|[110]$); (b) and (c) excitation of the $M=+1$ and $M=-1$ components, respectively (laser polarization $\vec{e}_L\|[1\bar{1}0]$).

volving more than a single acoustic phonon, leading to a thermalization of the exciton population and hence to a line broadening, and (iii) the 3D character of the scattering leading to changes in line shape, which would require an elaborate treatment, outside of the scope of this paper.

The line shape of the fine structure is defined by the selection rules for emission from each specific component. The height of each gray area in the plots of Fig. 3 corresponds to the calculated oscillator strength of the corresponding transition, according to Table I. Again, qualitative agreement is obtained. It should be noted that the mixing of the $\Gamma_5^+$ components due to the $k^2$-exchange terms, the density of states of the final state and thermalization effects, which might lead to a broad background, are not taken into account. This could explain part of the discrepancies observed between theoretical and experimental values of oscillator strength.

Figure 4 shows the resonant Raman spectra of the $\Gamma_4^-$ phonons at 5 T for excitation in the $M=0$, $\pm1$ components. The *L*-*T* splitting and the shifts in magnetic field are clearly resolved. The polarization selection rules of Table I ($\vec{B}\|[110]$ and $\vec{k}\|[001]$) are confirmed, except for the intensity ratio of the LO to TO resonances. According to Table I, it is expected to be 1 for the $\pm1$ components as compared to almost 2 in the experiments. This might be due to Fröhlich electron-phonon interaction for LO phonons as already discussed in Ref. 1. It is worth noting that the number of additional features induced by acoustic phonons decreases on moving the excitation from the $M=+1$ to the $M=-1$ component, since Stokes processes involving lower-lying components are dominating at this temperature ($kT\approx120$ $\mu$eV) due to the large energy separation of the components at 5 T ($E_{5T}^{+1}-E_{5T}^{-1}=480$ $\mu$eV).

Up to now excitons have been considered to be scattered mostly by LO and LA phonons,[1,17] whereas intraband scattering dominates over interband scattering.[17] Our experiment, instead, clearly shows both a pronounced participation of TA phonons and an enhanced fast interband coupling, also mediated by LA phonons. In the present experiment in Voigt configuration with $\vec{B}\|[110]$, the contribution of LA (TA) phonons to interband (intraband) scattering processes arises due to the symmetry of the exciton-phonon coupling operator, which contains $\Gamma_3^+$ ($\Gamma_5^+$) components enabling these transitions in this geometry.[17] In any case, the enhanced probability of TA scattering processes with respect to LA-mediated processes still remains to be explained, as well as the efficiency of two-phonon scattering processes. At first sight, two main differences may be envisaged between previous experiments and ours: (i) the application of a magnetic field splits the orthoexciton components, allowing to resolve a rich dynamics, while previous measurements[1,2] were done at $B=0$ T; (ii) the *resonant* nature of the exciting photons and the *real* nature of the intermediate states populated via acoustic phonons might lead to a fast and efficient relaxation via TA phonons and eventually to stimulation effects.

## V. CONCLUSIONS

In conclusion, we have performed resonant Raman and luminescence spectroscopy on the lowest $M=0$ and $M=\pm1$ orthoexciton components of bulk $Cu_2O$ in a magnetic field. Depending on crystal orientation and polarization of the outgoing light, $\Gamma_3^-$, $\Gamma_4^-$, and $\Gamma_5^-$ optical phonon replicas have been analyzed, which show a pronounced fine structure. We ascribe these additional structures to LA- and TA-mediated intraband and interband scattering processes among orthoexciton components, which are split by a magnetic field. This is in contrast to the general opinion that excitons are dominantly scattered by LA phonons and intraband scattering is dominating interband scattering.[17] We relate this to the *d*-like character of the valence band in $Cu_2O$ with rather strong shear deformation potentials.[18] The study of acoustic phonon interaction is of importance for understanding of exciton relaxation processes into a possible Bose condensed exciton state. As an outlook on further investigations of $Cu_2O$ we mention Raman scattering of the paraexciton in a magnetic field. The detailed study of intraband LA scattering should allow to determine the effective mass of the paraexciton which is not affected by the $k^2$-exchange terms.

## ACKNOWLEDGMENTS

We acknowledge support by the Deutsche Forschungsgemeinschaft (Graduiertenkolleg "Materialeigenschaften und Konzepte für die Quanteninformationsverarbeitung," and "Quantum Optics in Semiconductors" Research Group).

*Present address: School of Physics and Astronomy, University of Southampton, Southampton, SO17 1BJ, U.K.
†Electronic address: dietmar.froehlich@physik.uni-dortmund.de

[1] A. Z. Genack, H. Z. Cummins, M. A. Washington, and A. Compaan, Phys. Rev. B **12**, 2478 (1975).
[2] P. Y. Yu and Y. R. Shen, Phys. Rev. B **12**, 1377 (1975); **17**, 4017 (1978); P. Y. Yu, in *Excitons*, edited by K. Cho, Topics in Current Physics Vol. 14 (Springer-Verlag, Berlin, 1979), p. 211.
[3] C. Ell, A. L. Ivanov, and H. Haug, Phys. Rev. B **57**, 9663 (1998).
[4] R. G. Ulbrich and C. Weisbuch, Phys. Rev. Lett. **38**, 865 (1977); Adv. Solid State Phys. **18**, 217 (1978).
[5] V. C. Y. So, M. Fukui, P. J. Thomas, and G. I. Stegeman, J. Phys. C **14**, 4505 (1981).
[6] J. L. Birman, Phys. Rev. B **9**, 4518 (1974).
[7] G. Dasbach, D. Fröhlich, H. Stolz, R. Klieber, D. Suter, and M. Bayer, Phys. Rev. Lett. **91**, 107401 (2003); G. Dasbach, D. Fröhlich, R. Klieber, D. Suter, M. Bayer, and H. Stolz, Phys. Rev. B **70**, 045206 (2004).
[8] G. Baldassarri Höger von Högersthal, G. Dasbach, D. Fröhlich, M. Kulka, H. Stolz, and M. Bayer, J. Lumin. **112**, 25 (2005).
[9] G. Kuwabara, M. Tanaka, and H. Fukutani, Solid State Commun. **21**, 599 (1977).
[10] D. Fröhlich and R. Kenklies, Phys. Status Solidi B **111**, 247 (1982).
[11] G. Dasbach, D. Fröhlich, H. Stolz, R. Klieber, D. Suter, and M. Bayer, Phys. Status Solidi C **2**, 886 (2005).
[12] D. Fröhlich, G. Dasbach, G. Baldassarri Höger von Högersthal, M. Bayer, R. Klieber, D. Suter, and H. Stolz, Solid State Commun. **134**, 139 (2005).
[13] G. F. Koster, J. O. Dimmock, R. G. Wheeler, and H. Statz, *Properties of the Thirty-Two Point Groups* (MIT Press, Cambridge, MA, 1963).
[14] In principle the TA phonon in the $[1\bar{1}0]$ direction is split into two components with slightly different $v_{TA}$ as measured by M. M. Beg and S. M. Shapiro, Phys. Rev. B **13**, 1728 (1976).
[15] K. Huang, Z. Phys. **171**, 213 (1963); C. Carabatos, Phys. Status Solidi **37**, 773 (1970); C. Carabatos and B. Prevot, Phys. Status Solidi B **44**, 701 (1971).
[16] K. Reimann and K. Syassen, Phys. Rev. B **39**, 11113 (1989).
[17] P. Y. Yu and M. Cardona, *Fundamentals of Semiconductors: Physics and Materials Properties* (Springer-Verlag, Berlin, 1996).
[18] R. G. Waters, F. H. Pollak, R. H. Bruce, and H. Z. Cummins, Phys. Rev. B **21**, 1665 (1980); H.-R. Trebin, H. Z. Cummins, and J. L. Birman, *ibid.* **23**, 597 (1981).